

Minority anion substitution by Ni in ZnO

L. M. C. Pereira, U. Wahl, J. G. Correia, L. M. Amorim, D. J. Silva, E. Bosne, S. Decoster, M. R. da Silva, K. Temst, and A. Vantomme

Citation: [Applied Physics Letters](#) **103**, 091905 (2013); doi: 10.1063/1.4820254

View online: <http://dx.doi.org/10.1063/1.4820254>

View Table of Contents: <http://scitation.aip.org/content/aip/journal/apl/103/9?ver=pdfcov>

Published by the [AIP Publishing](#)

Articles you may be interested in

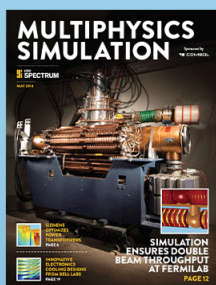
[Structural, optical, vibrational, and magnetic properties of sol-gel derived Ni doped ZnO nanoparticles](#)
J. Appl. Phys. **114**, 033912 (2013); 10.1063/1.4813868

[Correlation between microstructural and magnetic properties of Tb implanted ZnO](#)
AIP Conf. Proc. **1525**, 300 (2013); 10.1063/1.4802337

[Probing origin of room temperature ferromagnetism in Ni ion implanted ZnO films with x-ray absorption spectroscopy](#)
J. Appl. Phys. **111**, 013715 (2012); 10.1063/1.3676260

[Photoluminescence studies on structural defects and room temperature ferromagnetism in Ni and Ni-H doped ZnO nanoparticles](#)
J. Appl. Phys. **108**, 023906 (2010); 10.1063/1.3460644

[Doping concentration dependence of room-temperature ferromagnetism for Ni-doped ZnO thin films prepared by pulsed-laser deposition](#)
Appl. Phys. Lett. **88**, 062508 (2006); 10.1063/1.2170420



Free online magazine

MULTIPHYSICS SIMULATION

READ NOW ►

 COMSOL

Minority anion substitution by Ni in ZnO

L. M. C. Pereira,^{1,a)} U. Wahl,² J. G. Correia,² L. M. Amorim,¹ D. J. Silva,³ E. Bosne,^{2,4} S. Decoster,¹ M. R. da Silva,⁵ K. Temst,¹ and A. Vantomme¹

¹*Instituut voor Kern-en Stralingsfysica, KU Leuven, 3001 Leuven, Belgium*

²*Campus Tecnológico e Nuclear, Instituto Superior Técnico, Universidade de Lisboa, 2686-953 Sacavém, Portugal*

³*IFIMUP and IN-Institute of Nanoscience and Nanotechnology, Universidade do Porto, 4169-007 Porto, Portugal*

⁴*Department of Materials and Ceramics Engineering and CICECO, University of Aveiro, 3810-193 Aveiro, Portugal*

⁵*Centro de Física Nuclear da Universidade de Lisboa, 1649-003 Lisboa, Portugal*

(Received 20 July 2013; accepted 21 August 2013; published online 30 August 2013)

We report on the lattice location of implanted Ni in ZnO using the β^- emission channeling technique. In addition to the majority substituting for the cation (Zn), a significant fraction of the Ni atoms occupy anion (O) sites. Since Ni is chemically more similar to Zn than it is to O, the observed O substitution is rather puzzling. We discuss these findings with respect to the general understanding of lattice location of dopants in compound semiconductors. In particular, we discuss potential implications on the magnetic behavior of transition metal doped dilute magnetic semiconductors. © 2013 AIP Publishing LLC. [<http://dx.doi.org/10.1063/1.4820254>]

Despite being extensively investigated for more than ten years, the existence of *intrinsic* room-temperature ferromagnetism in wide-gap dilute magnetic semiconductors (DMS), such as 3d transition-metal doped ZnO and GaN, remains a topic of intense debate.^{1,2} ZnO doped with Ni (either during growth^{3,4} or by ion implantation^{5–8}) is a good example of that, with similar magnetic behavior being ascribed to intrinsic ferromagnetic order in some cases,^{3,5,6} and ferromagnetic secondary phases in others.^{4,7,8}

Since the magnetic behavior of a specific dopant-host combination is largely dependent on the material's local structure, the precise determination of the dopants' lattice location is crucial for the understanding of DMS materials. In ZnO doped with Ni (high doping regime, i.e., few atomic %) either during growth^{9–11} or by ion implantation,⁶ Ni has been found to substitute only the cation (Zn), based on extended X-ray absorption fine structure (XAFS) experiments.^{6,9–11} Making use of β^- emission channeling, we have also observed *pure* Zn substitution by 3d transition metals, namely, Fe (Ref. 12) and Cu,¹³ in the very dilute regime (<0.02 at. %). However, for other 3d transition metals (Mn and Co), also in the very dilute regime, we have recently observed minority O substitution (~20%),¹⁴ which is remarkably unexpected based on the general understanding of lattice site preference of impurities in compound semiconductors. Such a dependence on transition metal impurity, without an obvious trend across the 3d series—for example, a clear dependence on atomic number Z : Mn ($Z=25$), Fe (26), Co (27), Cu (29)—suggests the existence of an intricate underlying mechanism which is yet to be understood. Crucial for the formulation of such a mechanism is a comprehensive investigation of the conditions under which anion substitution occurs, in particular, regarding which transition-metal/host combinations can accommodate it.

Here, we report on β^- emission channeling studies of the lattice location of implanted Ni ($Z=28$) in ZnO, in the very dilute regime (<0.02 at. %). Emission channeling¹⁵ makes use of the charged particles emitted by a decaying radioactive isotope. The screened Coulomb potential of atomic rows and planes determines the anisotropic scattering of the particles emitted isotropically during decay. Since these channeling and blocking effects strongly depend on the initial position of the emitted particles, they result in angular emission patterns around major crystallographic axes which are characteristic of the lattice sites occupied by the probe atoms. As radioactive probe, we used ⁶⁵Ni ($t_{1/2}=2.5$ h), which has recently become available at the on-line isotope separator facility ISOLDE at CERN. ⁶⁵Ni is produced by means of 1.4 GeV proton-induced fission from uranium carbide targets, and following outdiffusion from the target and element-specific ionization by means of a laser ion source,^{16,17} is available as an isotopically pure ion beam. The ⁶⁵Ni nuclei decay to stable ⁶⁵Cu by means of β^- emission with an endpoint energy of 2.137 MeV and an average β^- energy of 629 keV. A commercially available ZnO wurtzite [0001] single-crystal (CrysTec GmbH), hydrothermally grown and Zn-face polished, was implanted at room temperature with a fluence of $2 \times 10^{13} \text{ cm}^{-2}$ of ⁶⁵Ni. The implantation was performed under a tilt angle of 17° to minimize ion channeling, using an energy of 50 keV, resulting in a peak concentration of $7.0 \times 10^{18} \text{ cm}^{-3}$ (0.017 at. %) at a projected range of 231 Å with a 109 Å straggling, as estimated using SRIM.¹⁸ In this low concentration regime, phase segregation and extended beam induced disorder are minimized, both of which occur for Ni concentrations in the atomic % range^{6,8} (discussed in more detail below). Angular-dependent emission yields of the β^- particles were measured at room temperature along four crystallographic directions, [0001], $[\bar{1}102]$, $[\bar{1}101]$, and $[\bar{2}113]$, in the as-implanted state and after *in situ* capless annealing in vacuum (< 10^{-5} mbar) at 300 °C, 600 °C, and 900 °C. These patterns were recorded

^{a)}lino.pereira@fys.kuleuven.be

using a position- and energy-sensitive detection system similar to that described in Ref. 19. Given the short half-life of ^{65}Ni , this system was installed on-line and upgraded with self-triggering readout chips for the Si pad detectors, enabling measurements during and/or immediately after implantation with count rates of up to several kHz.²⁰

Quantitative lattice location is provided by fitting the two-dimensional experimental patterns with theoretical ones using the fit procedure outlined in Ref. 21. The theoretical patterns were calculated using the *manybeam* formalism¹⁵ for probes occupying various sites in the wurtzite ZnO structure:²² substitutional Zn (S_{Zn}) and O (S_{O}) sites with varying root-mean-square displacements, the main interstitial sites, i.e., tetrahedral (T), octahedral (O), hexagonal (H), bond-centered (BC), and anti-bonding (AB), as well as interstitial sites resulting from displacements along the c or the basal directions. For all four measured directions, the calculated S_{Zn} patterns gave by far the best agreement, showing that the majority of the probe atoms occupy S_{Zn} sites, as expected. The fitting routine was then allowed to include, in addition to S_{Zn} , an additional lattice site, for which all simulated sites were considered. Consistently, for all measured directions, the $S_{\text{Zn}} + S_{\text{O}}$ double occupancy gave the best fit compared to all other combinations, and considerably improves the S_{Zn} single-site fit, with up to 25% lower reduced χ^2 . This is illustrated in Fig. 1, showing the reduced χ^2 of the fit as the non- S_{Zn} site is moved along the c -axis between two neighboring S_{Zn} sites (these sites are indistinguishable along the [0001] direction, which is therefore not included). Consistently, for all three directions, the best fits are centered at the S_{O} site. The sensitivity of the fit (in terms of magnitude and “width” of the improvement in χ^2) is correlated with the spatial separation between Zn and O rows along the channeling axis (depicted in the bottom right hand corner of Fig. 1), being

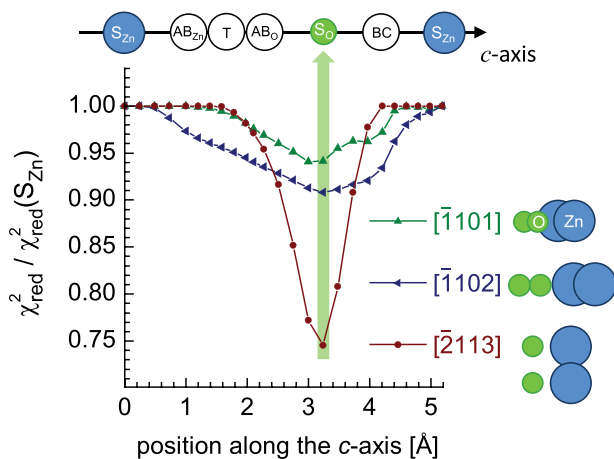


FIG. 1. Reduced χ^2 of the fits to the experimental emission yields in the vicinity of the $[1102]$, $[1101]$, and $[2113]$ directions (following 300°C annealing). Each data point corresponds to the best fit obtained using two given sites, with the corresponding two fractions as free parameters. The site pairs are composed of S_{Zn} plus each of the simulated sites along the c -axis (depicted above the plot): the S_{O} and the T sites, the BC and AB sites along the c -axis, and a number of intermediate positions. The x -axis corresponds to the position (along the c -axis) of the non- S_{Zn} site used in each fit. The reduced χ^2 (y -axis) of these two-site fits are normalized to that of the one-site (S_{Zn}) fit. The non-equivalent rows of Zn and O atoms, projected on the plane perpendicular to each of the axes, are also shown (right). Note that the separation between Zn and O rows is maximized along the $[2113]$ axis.

most pronounced for the $[2113]$ direction. The good match between experiment and simulated patterns is illustrated in Fig. 2 which compares the normalized experimental β^- emission yields following annealing at 300°C along the four measured directions [(a)–(d)] with the best fits of theoretical patterns [(e)–(h)]. The best fit is obtained for 79% of the ^{65}Ni atoms on S_{Zn} (Ni_{Zn}) and 21% on S_{O} sites (Ni_{O}). Introducing a third site yields only insignificant fit improvements. Possible fractions in other sites are estimated to be below 5%. Figure 3 summarizes the output of the fitting procedure, i.e., the fractions of ^{65}Ni probes in S_{Zn} and S_{O} sites as a function of annealing temperature. Within the experimental error, the Ni_{O} fraction remains constant around 20%, up to the highest annealing temperature of 900°C .

In compound semiconductors, chemical similarities between impurity and host elements usually determine the preferred lattice site and hence all the magnetic (e.g., Fe_{Zn}),¹² electric (e.g., In_{Zn}),²³ and optical (e.g., Er_{Zn})²⁴ properties of impurities. Therefore, the observed anion (O) substitution by a transition metal impurity, such as Ni, is rather unexpected, since the electronegativity and ionic radii of Ni are much closer to those of Zn than of O. In the previous lattice location studies on ZnO thin films doped during growth (high doping regime, i.e. few atomic %), the XAFS spectra have been satisfactorily fitted with pure Zn substitution (e.g., Refs. 9 and 10). Lattice location studies on Ni-implanted

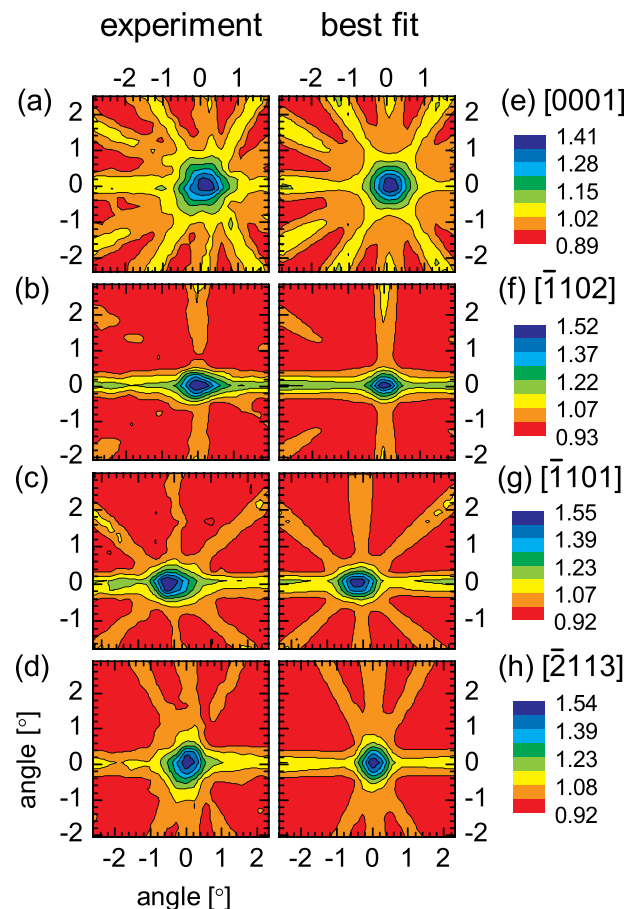


FIG. 2. (a)–(d) Normalized experimental ^{65}Ni β^- emission channeling patterns in the vicinity of the $[0001]$, $[1102]$, $[1101]$, and $[2113]$ directions following annealing at 300°C . (e)–(h) Corresponding best fits with 21% and 79% of the ^{65}Ni atoms on S_{Zn} and S_{O} sites, respectively.

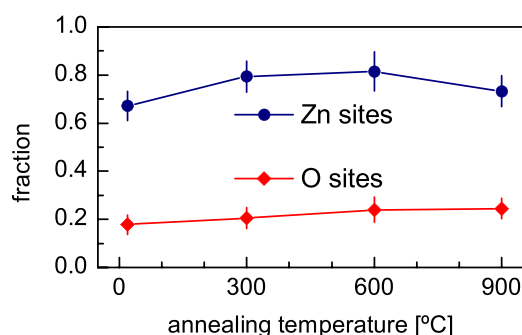


FIG. 3. Fractions of ^{65}Ni impurities on S_{Zn} and S_{O} sites following each annealing step.

ZnO are very scarce, especially in the low concentration regime studied here. In the high concentration regime, precise lattice location is hindered by the highly disordered surroundings of the Ni impurities. For example, in ZnO thin films implanted with Ni to concentrations of 1–10 at. %, the majority of the Ni atoms are located in regions so heavily disturbed that the local wurtzite environment is lost,⁶ making it also difficult to identify (or even define) any lattice site (including O-substitutional sites). Relevant for this discussion is also the reported segregation of Co into intermetallic CoZn inclusions in Co-doped ZnO (high Co doping regime, during thin film growth), detected by XAFS.²⁵ In principle, if a similar NiZn phase would form, it could potentially lead to a fitted Ni_O fraction. However, these intermetallic phases are incommensurate with the ZnO wurtzite structure. Therefore, even if a large fraction of the Ni impurities would have segregated into such phases, only a very small fraction would be aligned with the axes containing the O sites (simultaneously along the four measured crystallographic directions), and the majority of the Ni impurities would actually be located in poorly aligned sites (i.e., would contribute with a *random* fraction). This scenario is inconsistent with our data, since virtually all the Ni (within an experimental uncertainty of a few %) is located in high-symmetry Zn and O sites. Furthermore, such pronounced segregation (>20% of the Ni impurities) is extremely unlikely to occur in our case, given the very low Ni concentration and the fact that the Ni_O fraction is observed after implantation at room temperature (i.e., even before high-temperature annealing).

Despite being very unexpected, O substitution by Ni in ZnO is in line with our previous reports of minority anion substitution by implanted Mn and Co in ZnO (Ref. 14) as well as Mn in GaN (Ref. 26) (GaN is closely related to ZnO in crystal structure, bandgap, defect chemistry, ...). The non-equilibrium nature of ion implantation (used here and in Refs. 14 and 26) may play a favorable role, since the high concentration of O vacancies created upon implantation is likely to facilitate impurity incorporation in O sites. However, such argumentation does not explain why, under very similar experimental conditions, anion substitution does *not* occur for Fe (Ref. 12) and Cu (Ref. 13) (Mn, Fe, Co, Ni, and Cu are all 3d transition metals, with a similar atomic mass, and therefore, similar incorporation kinetics). A particularly interesting case to compare to the observed anion substitution (i.e., substitution of other than the expected host element) are group V impurities (e.g., As and Sb) in ZnO.

These impurities are considered as potential *p*-type dopants if substituting for O. However, we have previously shown that, instead, As (Ref. 27) and Sb (Ref. 28) substitute for Zn, i.e., contrary to what one would expect from their position in the periodic table. The Zn-site character of As and Sb can, in principle, be explained by the large size mismatch of As^{3+} and Sb^{3+} with O^{2+} but the good match with Zn^{2+} , by the match of electronegativity, and by their character as semimetals.^{27,28} However, none of these arguments help explaining the observed minority O substitution by transition metals, on the contrary. As mentioned above, the electronegativity and ionic radii of Ni are much closer to those of Zn than of O and, in addition, 3d transition metals are chemically more similar to post-transition metals such as Zn than to non-metals such as O. In fact, the observed O substitution is so unexpected that theoretical considerations of the phenomenon are very limited. The case that has been considered theoretically which most resembles anion-substitutional transition metals is the Zn antisite (Zn_O). Depending on the growth conditions (Zn- or O-rich) and Fermi level, Zn_O charge states of up to 4^+ have been predicted to be stable, with the $2^+/3^+$ and $3^+/4^+$ levels lying deep in the bandgap.^{29–32} Interestingly, the formation energy of Zn_O^{4+} can be very small, even negative, under metal-rich conditions and for a Fermi level close to the valence band maximum. Therefore, granted that the $3^+/4^+$ levels of Mn_O , Co_O , and Ni_O lie above the Fermi level, it is conceivable that the formation energies of such defects may indeed be small enough to allow for sizable concentrations. Conversely, if the $3^+/4^+$ levels of Fe_O and Cu_O lie deeper in the bandgap, below the Fermi level, such defects cannot form in significant concentrations (since the formation energy for the lower charge states can be expected to be larger^{29–32}). Such a selectivity mechanism would explain why we observed O substitution for some transition metals (Mn, Co, and Ni) and not for others (Fe and Cu). *Ab initio* density functional theory calculations similar to those reported for Zn_O in Refs. 29–32 could be used to verify if this scenario indeed applies. On the experimental side, a systematic (re)assessment of the lattice location of transition metals in ZnO and GaN for different preparation methods and growth conditions, carefully taking the possibility of anion substitution into consideration, would also greatly contribute to the understanding of the underlying physical mechanisms. A crucial step would consist of XAFS studies on a system for which our emission channeling measurements have shown anion substitution (Mn, Co, or Ni-implanted ZnO, or Mn-implanted GaN), prepared in identical conditions, i.e., 30–60 keV implantation, at room temperature, to a fluence of $\sim 2 \times 10^{13} \text{ cm}^{-2}$. Such studies would greatly complement our emission channeling results, by probing the local environment of anion-substitutional impurities, for example, in terms of the role played by other point defects such as anion or cation vacancies. Such a detailed description of the impurity lattice site and local environment, obtained from the combination of emission channeling and XAFS measurements, would then greatly simplify the theoretical assessment of anion substitution phenomena, for example, in the form of the *ab initio* calculations mentioned above (by narrowing down the otherwise numerous possible defect configurations).

Regarding the effect of minority anion-site substitution on the magnetic behavior of wide-gap DMS materials, although it has never been considered theoretically before, one can argue that it is more likely to negatively affect eventual mechanisms of ferromagnetic interaction. For example, in Mn-doped GaN, the type of magnetic interactions between Mn_{Ga} moments is charge state dependent.³³ Since anion-substitutional transition metals are most likely donor defects, as suggested above, Mn_{N} may convert ferromagnetically interacting $\text{Mn}_{\text{Ga}}^{3+}$ into antiferromagnetically interacting $\text{Mn}_{\text{Ga}}^{2+}$, as has been described for other donor defects.³³ These effects are likely to be general to transition metal doped ZnO, GaN and even other dilute magnetic semiconductors. Conceptually, such a (self-)compensation mechanism by minority anion-substitutional transition metals is similar to that of interstitial Mn in GaAs,^{34,35} also a donor which compensates acceptor and ferromagnetically interacting Ga-substitutional Mn.³⁶

In summary, we have experimentally determined the lattice location of implanted Ni in ZnO in the low concentration regime (<0.02 at. %). In addition to the majority on substitutional Zn sites, approximately 20% of the implanted Ni atoms were found to occupy O sites. Both Zn- and O-substitutional fractions were virtually unaffected by thermal annealing up to 900 °C. Being difficult to reconcile with the established scenario of pure cation substitution, these findings raise two fundamental questions: (1) What mechanism determines that, under similar doping conditions, some transition-metal/host combinations accommodate minority anion substitution and others do not? (2) How does minority anion substitution affect the magnetic properties of dilute magnetic semiconductors?

This work was supported by the Portuguese Foundation for Science and Technology (CERN/FP/123585/2011 and SFRH/BD/35761/2007), the European Union Seventh Framework through ENSAR (European Nuclear Science and Applications Research, Contract No. 262010) and SPIRIT (Support of Public and Industrial Research Using Ion Beam Technology, Contract No. 227012), the Fund for Scientific Research-Flanders (FWO), and the Concerted Action of the KU Leuven (GOA/2009/006 and GOA/14/007).

¹T. Dietl, *Nature Mater.* **9**, 965 (2010).

²L. M. C. Pereira, J. P. Araujo, U. Wahl, S. Decoster, M. J. Van Bael, K. Temst, and A. Vantomme, *J. Appl. Phys.* **113**, 023903 (2013).

³W. Yu, L. H. Yang, X. Y. Teng, J. C. Zhang, Z. C. Zhang, L. Zhang, and G. S. Fu, *J. Appl. Phys.* **103**, 093901 (2008).

⁴M. Snure, D. Kumar, and A. Tiwari, *Appl. Phys. Lett.* **94**, 012510 (2009).

⁵B. Pandey, S. Ghosh, P. Srivastava, P. Kumar, and D. Kanjilal, *J. Appl. Phys.* **105**, 033909 (2009).

⁶P. Srivastava, S. Ghosh, B. Joshi, P. Satyarthi, P. Kumar, D. Kanjilal, D. Buerger, S. Zhou, H. Schmidt, A. Rogalev, and F. Wilhelm, *J. Appl. Phys.* **111**, 013715 (2012).

⁷M. Schumm, M. Koerdel, S. Mueller, C. Ronning, E. Dynowska, Z. Golacki, W. Szuszkiewicz, and J. Geurts, *J. Appl. Phys.* **105**, 083525 (2009).

⁸S. Zhou, K. Potzger, J. von Borany, R. Groetzschel, W. Skorupa, M. Helm, and J. Fassbender, *Phys. Rev. B* **77**, 035209 (2008).

⁹B. B. Li, X. Q. Xiu, R. Zhang, Z. K. Tao, L. Chen, Z. L. Xie, Y. D. Zheng, and B. He, *Chin. Phys. Lett.* **23**, 907 (2006).

¹⁰B. B. Li, X. Q. Xiu, R. Zhang, Z. K. Tao, L. Chen, Z. L. Xie, Y. D. Zheng, and Z. Xie, *Mater. Sci. Semicond. Process.* **9**, 141 (2006).

¹¹J. J. Lu, T. C. Lin, S. Y. Tsai, T. S. Mo, and K. J. Gan, *J. Magn. Magn. Mater.* **323**, 829 (2011).

¹²E. Rita, U. Wahl, J. G. Correia, E. Alves, and J. C. Soares, *Appl. Phys. Lett.* **85**, 4899 (2004).

¹³U. Wahl, E. Rita, J. G. Correia, E. Alves, and J. C. Soares, *Phys. Rev. B* **69**, 012102 (2004).

¹⁴L. M. C. Pereira, U. Wahl, S. Decoster, J. G. Correia, L. M. Amorim, M. R. da Silva, J. P. Araujo, and A. Vantomme, *Phys. Rev. B* **84**, 125204 (2011).

¹⁵H. Hofsaess and G. Lindner, *Phys. Rep.* **201**, 121 (1991).

¹⁶V. N. Fedosseev, L. E. Berg, N. Lebas, O. J. Launila, M. Lindroos, R. Losito, B. A. Marsh, F. K. Osterdahl, T. Pauchard, G. Transtromer, and J. Vannesjo, *Nucl. Instrum. Methods Phys. Res. B* **266**, 4378 (2008).

¹⁷V. N. Fedosseev, Y. Kudryavtsev, and V. I. Mishin, *Phys. Scr.* **85**, 058104 (2012).

¹⁸J. F. Ziegler, M. D. Ziegler, and J. P. Biersack, *Nucl. Instrum. Methods Phys. Res. B* **268**, 1818 (2010).

¹⁹U. Wahl, J. G. Correia, A. Czermak, S. G. Jahn, P. Jalocha, J. G. Marques, A. Rudge, F. Schopper, J. C. Soares, A. Vantomme, P. Weillhammer, and ISOLDE collaboration, *Nucl. Instrum. Methods Phys. Res. A* **524**, 245 (2004).

²⁰M. R. Silva, U. Wahl, J. G. Correia, L. M. Amorim, and L. M. C. Pereira, *Rev. Sci. Instrum.* **84**, 073506 (2013).

²¹U. Wahl, J. G. Correia, S. Cardoso, J. G. Marques, A. Vantomme, G. Langouche, and ISOLDE collaboration, *Nucl. Instrum. Methods Phys. Res. B* **136**, 744 (1998).

²²U. Wahl, A. Vantomme, G. Langouche, J. P. Araujo, L. Peralta, J. G. Correia, and ISOLDE collaboration, *J. Appl. Phys.* **88**, 1319 (2000).

²³T. Agne, M. Deicher, V. Koteski, H. E. Mahnke, H. Wolf, and T. Wichert, *Hyperfine Interact.* **159**, 55 (2004).

²⁴U. Wahl, E. Rita, J. G. Correia, E. Alves, J. P. Araujo, and ISOLDE collaboration, *Appl. Phys. Lett.* **82**, 1173 (2003).

²⁵S. M. Heald, T. Kaspar, T. Droubay, V. Shutthanandan, S. Chambers, A. Mokhtari, A. J. Behan, H. J. Blythe, J. R. Neal, A. M. Fox, and G. A. Gehring, *Phys. Rev. B* **79**, 075202 (2009).

²⁶L. M. C. Pereira, U. Wahl, J. G. Correia, S. Decoster, L. M. Amorim, M. R. da Silva, J. P. Araujo, and A. Vantomme, *Phys. Rev. B* **86**, 195202 (2012).

²⁷U. Wahl, E. Rita, J. G. Correia, A. C. Marques, E. Alves, J. C. Soares, and ISOLDE collaboration, *Phys. Rev. Lett.* **95**, 215503 (2005).

²⁸U. Wahl, J. G. Correia, T. Mendonca, and S. Decoster, *Appl. Phys. Lett.* **94**, 261901 (2009).

²⁹A. Janotti and C. G. Van de Walle, *Phys. Rev. B* **76**, 165202 (2007).

³⁰F. Oba, A. Togo, I. Tanaka, J. Paier, and G. Kresse, *Phys. Rev. B* **77**, 245202 (2008).

³¹F. Oba, M. Choi, A. Togo, A. Seko, and I. Tanaka, *J. Phys.: Condens. Matter* **22**, 384211 (2010).

³²R. Vidya, P. Ravindran, H. Fjellvag, B. G. Svensson, E. Monakhov, M. Ganchenkova, and R. M. Nieminen, *Phys. Rev. B* **83**, 045206 (2011).

³³A. Bonanni, M. Sawicki, T. Devillers, W. Stefanowicz, B. Faina, T. Li, T. E. Winkler, D. Sztienkiel, A. Navarro-Quezada, M. Rovezzi, R. Jakiela, A. Grois, M. Wegscheider, W. Jantsch, J. Suffczynski, F. D'Acapito, A. Meingast, G. Kothleitner, and T. Dietl, *Phys. Rev. B* **84**, 035206 (2011).

³⁴L. M. C. Pereira, U. Wahl, S. Decoster, J. G. Correia, M. R. da Silva, A. Vantomme, and J. P. Araujo, *Appl. Phys. Lett.* **98**, 201905 (2011).

³⁵L. M. C. Pereira, U. Wahl, S. Decoster, J. G. Correia, L. M. Amorim, M. R. da Silva, J. P. Araujo, and A. Vantomme, *Phys. Rev. B* **86**, 125206 (2012).

³⁶T. Jungwirth, K. Y. Wang, J. Masek, K. W. Edmonds, J. König, J. Sinova, M. Polini, N. A. Goncharuk, A. H. MacDonald, M. Sawicki, A. W. Rushforth, R. P. Campion, L. X. Zhao, C. T. Foxon, and B. L. Gallagher, *Phys. Rev. B* **72**, 165204 (2005).